Variational path-integral theory of thermal properties of solids

Shudun Liu and G. K. Horton
Serin Physics Laboratory, Rutgers University, P.O. Box 849, Piscataway, New Jersey 08855-0849

E. R. Cowley
Department of Physics, Camden College of Arts and Science, Rutgers University, Camden, New Jersey 08102-1205
(Received 29 March 1991)

We show that the Feynman path-integral formulation of the quantum many-body problem, when combined with a quadratic trial action whose parameters are determined variationally, leads to a partition function with a temperature- and volume-dependent effective potential that can easily be evaluated by the classical Monte Carlo method. This leads directly to reliable thermal properties of solids over a wide range of volumes and temperatures. To demonstrate the power of this theory, we apply it to Mie–Lennard-Jones crystals. We compare the results systematically with predictions of anharmonic and self-consistent lattice dynamics as well as classical Monte Carlo calculations. The results of this theory agree with the former ones, where they are applicable, for a wide range of volumes and from $T=0$ K to melting. This method should be regarded as an alternative to the quantum Monte Carlo approach for most quantum solids, since it is reliable and requires much less computer time.

I. INTRODUCTION

To calculate the thermodynamic properties of solids is an old problem. Despite the development of a variety of theories, it remains difficult to account for both quantum effects and anharmonic vibrations. Lattice dynamical theories,[1] based on the expansion of atomic vibrations about their equilibrium positions, generally are valid at low temperatures, where these vibrations are small. They fail at high temperatures when the atomic vibrations get larger and larger and more anharmonic. To deal with the large thermal anharmonic vibrations, one can use classical Monte Carlo (CMC) or molecular dynamics (MD) techniques. Since CMC and MD are based on Newton's laws, they cannot account for quantum effects. So they are not applicable at low temperatures when quantum effects become important. The relevant temperature here is Θ_D (the Debye temperature) below which quantum effects are important, and CMC and MD are no longer reliable. With the Wigner expansion,[2] CMC, for example, can be applied down to temperatures around the Debye temperature. The Wigner expansion is in terms of h/T, so it is clear that it cannot work at low temperatures.

Thus we face the fact that, generally speaking, we have theories for low temperatures and theories for high temperatures, but we do not have one that works at all temperatures. This temperature gap, where no theories work, depends on the kind of material being studied. Since perturbation theories work up to roughly half of T_m (the melting temperature) and CMC is applicable down to about Θ_D, we can get a fairly good idea of the gap for a specific material by looking at its T_m and Θ_D. If T_m is very large compared with Θ_D, then the gap is very small and existing theories will overlap. On the other hand, if T_m is comparable with Θ_D or in some cases it is even less than Θ_D, then there is a big gap.

Of course, self-consistent lattice dynamical theories were formulated[3] to remedy the deficiencies of lattice dynamics based on perturbation theory. These theories are particularly useful at low temperatures, $T<\Theta_D$. However, in this regime the reliability of self-consistent theories is hard to assay and they become rapidly more complicated when pushed to higher orders.[4] The present paper will give information on the reliability of one version of self-consistent lattice dynamics, namely, the improved self-consistent theory (ISC).[5]

It is clearly desirable to have a theory that works quantitatively at all temperatures. Such a theory must account for quantum effects at low temperatures as well as large thermal vibrations at high temperatures. We believe the recently proposed effective potential method[6,7] is a very promising candidate. This method is based on the Feynman variational path-integral theory. The Feynman path-integral form of the partition function is approximated by replacing the true action by a trial action. The trial action is of a quadratic form, so the path integration can be carried out analytically. The parameters in the trial action are then determined variationally using the well-known Feynman-Jensen inequality.[8] The path-integral form of the partition function then reduces to a classical partition function with the potential replaced by a temperature- and volume-dependent effective potential. This effective potential method has been applied to special problems, mostly particular cases of one-dimensional systems.[9] For this approach to be generally accepted, it is necessary to show that it is reliable for a wide variety of solids. This paper should be regarded as a step in that direction.

We have recently extended the effective potential method to a realistic three-dimensional solid.[10] Coupling this new method with the CMC technique, we calculated thermodynamic properties of solid Ar in order to investi-

gate whether the effective potential method does indeed work at all temperatures for a realistic three-dimensional solid. In this paper, we will study the thermal properties of Mie–Lennard-Jones (MLJ) solids in parameters appropriate to all inert gas solids (except solid He) in a systematic way. For the MLJ crystals there are many accurate numerical results of earlier theories available at high and low temperatures to provide a reliable check on our systematic calculations. We are well aware of the fact that reliable potentials describing the inert gas solids exist. But, before using these in our theory, we felt that we must be sure of its quantitative accuracy by making contact with corresponding earlier work. Also, from heavy solids such as Xe to the light members such as Ne, inert gas solids show a variety of quantum effects. We believe they provide an ideal system for which we can test the effective potential method.

In Sec. II, we will present the variational path-integral theory for a three-dimensional system. In Sec. III, we give the results for inert gas solids described by a nearest-neighbor MLJ potential.

II. THEORY

Since the full three-dimensional theory used in this paper has not been presented in its complete generality, we present a summary here. We start with the Feynman path-integral form of the partition function

$$Z=e^{-\beta F}=\int\prod_{i=1}^{N}D\mathbf{r}_i(u)e^{-S[\mathbf{r}(u)]/\hbar}\ , \tag{1}$$

with $\mathbf{r}(u)=\{\mathbf{r}_1(u),\mathbf{r}_2(u),\ldots,\mathbf{r}_N(u)\}$, $\beta=1/k_BT$, where N is the number of atoms. The action S for a given potential is

$$S[\mathbf{r}(u)]=\int_0^{\beta\hbar}\left[\sum_{i=1}^{N}\tfrac{1}{2}m\dot{\mathbf{r}}_i^2(u)+V(\mathbf{r}(u))\right]du\ . \tag{2}$$

The integration variable u has the dimension of time. We use the following three-dimensional trial action,

$$S_0[\mathbf{r}(u)]=\int_0^{\beta\hbar}\left[\sum_{i=1}^{N}\tfrac{1}{2}m\dot{\mathbf{r}}_i^2(u)+W(\bar{\mathbf{r}})+\tfrac{1}{2}\sum_{i,j=1}^{N}[\mathbf{r}_i(u)-\bar{\mathbf{r}}_i]\cdot[\mathbf{r}_j(u)-\bar{\mathbf{r}}_j]\Omega_{ij}(\bar{\mathbf{r}})\right]du\ , \tag{3}$$

with $\bar{\mathbf{r}}\equiv\{\bar{\mathbf{r}}_1,\bar{\mathbf{r}}_2,\ldots,\bar{\mathbf{r}}_N\}$, where $\bar{\mathbf{r}}_i$ is the average point over each path so that

$$\bar{\mathbf{r}}_i=\frac{1}{\beta\hbar}\int_0^{\beta\hbar}\mathbf{r}_i(u)du\ . \tag{4}$$

In Eq. (3), $W(\bar{\mathbf{r}})$ is the potential at the average point of the path and $\Omega(\bar{\mathbf{r}})$ is a symmetric $N\times N$ matrix. Both are to be determined by the variational method. The last sum in Eq. (3) is not of the most general form possible, but has the advantage of simplicity in that each interaction is described by a single parameter. According to Eq. (3), a particle oscillates around the average point of its path in a harmonic way. This is a major improvement over Feynman's original approximation,[8] in which he neglected the last sum in Eq. (3). It is clear that our approximation will become better and better as the temperature increases. At high temperature, a particle has little "time($\beta\hbar$)" to travel, it can only oscillate around the average point of its path.

Since Ω_{ij} is a symmetric matrix, it can be diagonalized by an orthogonal matrix. Let U be such a matrix. One then has,

$$U_{ai}\Omega_{ij}U_{jb}^{-1}=m\omega_a^2\delta_{ab}\ , \tag{5}$$

where $m\omega_a^2$ are the eigenvalues of Ω.

After carrying out the path integral, we find

$$Z_0=e^{-\beta F_0}=\int\prod_{i=1}^{N}D\mathbf{r}_i(u)e^{-S_0[\mathbf{r}(u)]/\hbar}$$

$$=\int e^{-\beta W(\bar{\mathbf{r}})}\prod_{i=1}^{N}\left[d^3\bar{\mathbf{r}}_i\left[\frac{m}{2\pi\beta\hbar^2}\right]^{3/2}\frac{f_i(\bar{\mathbf{r}})}{\sinh f_i(\bar{\mathbf{r}})}\right] \tag{6}$$

and

$$\frac{1}{\beta}\langle S-S_0\rangle_0=\frac{1}{\beta Z_0}\int\prod_{i=1}^{N}D\mathbf{r}_i(u)(S-S_0)e^{-\frac{S_0[\mathbf{r}(u)]}{\hbar}}$$

$$=\int e^{-\beta W(\bar{\mathbf{r}})}\prod_{i=1}^{N}\left[d^3\bar{\mathbf{r}}_i\left[\frac{m}{2\pi\beta\hbar^2}\right]^{3/2}\frac{f_i(\bar{\mathbf{r}})}{\sinh f_i(\bar{\mathbf{r}})}\right]\left[K(\bar{\mathbf{r}})-W(\bar{\mathbf{r}})-\frac{3m}{\beta^2\hbar^2}\sum_{i=1}^{N}\alpha_i f_i^2\right], \tag{7}$$

where

$$K(\bar{\mathbf{r}})=\int V(U^T\boldsymbol{\eta}+\bar{\mathbf{r}})\prod_{i=1}^{N}\left[d^3\eta_i\frac{1}{\sqrt{\pi\alpha_i}}e^{-\eta_i^2/\alpha_i(\bar{\mathbf{r}})}\right] . \quad (8)$$

In Eqs. (6), (7), and (8), we have used the abbreviations

$$f_i=\tfrac{1}{2}\beta\hbar\omega_i , \quad (9)$$

and

$$\alpha_i=\frac{\beta\hbar^2}{2mf_i}(\coth f_i-1/f_i) . \quad (10)$$

The Feynman-Jensen inequality tells us that

$$F<F_0+\frac{1}{\beta}\langle S-S_0\rangle_0 . \quad (11)$$

The unknown parameters in Eq. (3) will be determined by minimizing the right-hand side of Eq. (11). Since the matrix Ω is determined by its eigenvalues and the U matrix, varying the matrix Ω is equivalent to varying ω_a^2 and U_{ab}.

From

$$\frac{\delta}{\delta W(\bar{\mathbf{r}})}\left[F_0+\frac{1}{\beta}\langle S-S_0\rangle\right]=0 , \quad (11')$$

one finds

$$W(\bar{\mathbf{r}})=K(\bar{\mathbf{r}})-\frac{3m}{\beta^2\hbar^2}\sum_{i=1}^{N}\alpha_i f_i^2 . \quad (12)$$

This leads to $\langle S-S_0\rangle_0=0$, and

$$Z_0=\int e^{-V_{\rm eff}(\bar{\mathbf{r}})}\prod_{i=1}^{N}\left[d^3\bar{\mathbf{r}}_i\left[\frac{m}{2\pi\beta\hbar^2}\right]^{3/2}\right] , \quad (13)$$

with

$$V_{\rm eff}(\bar{\mathbf{r}})=K(\bar{\mathbf{r}})-\frac{3m}{\beta^2\hbar^2}\sum_{i=1}^{N}\alpha_i f_i^2-\frac{3}{\beta}\sum_{i=1}^{N}\ln\left[\frac{f_i}{\sinh f_i}\right] . \quad (14)$$

Notice that Z_0 has the classical form with the potential V replaced by an effective potential, $V_{\rm eff}$. Finding the minimum of $V_{\rm eff}$ with respect to ω_a^2 and U_{ab}, one gets, after some algebra,

$$U_{ai}\tilde{K}_{ij}U_{jb}^T=\frac{12m}{\beta^2}f_a^2\delta_{ab} , \quad (15)$$

where

$$\tilde{K}_{ij}=\nabla_i\nabla_j K(\bar{\mathbf{r}}) . \quad (16)$$

So far, our formalism has been very general in the sense that we did not put any restriction on the interactions between particles. To simplify matters, we will now assume the potential has the two-body form

$$V(\mathbf{r})=\tfrac{1}{2}\sum_{i\neq j}v(\mathbf{r}_i-\mathbf{r}_j) . \quad (17)$$

For this potential, we find

$$K(\bar{\mathbf{r}})=\frac{1}{2}\sum_{L=0}^{\infty}\frac{1}{L!}\sum_{i\neq j}\left[\frac{D_{ij}}{2}\right]^L\Delta^{(L)}v(\bar{\mathbf{r}}_i-\bar{\mathbf{r}}_j) , \quad (18)$$

where $\Delta^{(L)}$ is the Lth power of the Laplacian operator. The quantum renormalization factor D_{ij} is defined to be

$$D_{ij}(\bar{\mathbf{r}})=\sum_{k=1}^{N}(U_{ki}-U_{kj})^2\frac{\alpha_k}{2} . \quad (19)$$

It is very difficult to solve the self-consistent equations (15), (16), (18), and (19) because they depend on the configurations of particles which are changing constantly. However, as long as the quantum fluctuations, as measured by the quantum renormalization factor D_{ij}, are small, one can expand these self-consistent equations around the equilibrium configurations. The validity of this kind of expansion will be discussed quantitatively later.

Let d_n be the distance between the nth neighbor particles at their equilibrium positions, h_n the number of the nth neighbors per particle. Then we find, at the equilibrium positions,

$$\tilde{K}_{ij}=\sum_{L=0}^{\infty}\frac{1}{L!}\sum_{n}\left[\frac{D_n}{2}\right]^L\Delta^{(L+1)}v(d_n)(h_n-b_{n,i,j}) , \quad (20)$$

where $b_{n,i,j}$ stands for the condition that particles a and b are the nth neighbors. For a one-dimensional chain, for example, one would have $h_1=2$, $b_{1,i,j}=\delta_{i,j+1}+\delta_{i,j-1}$, etc.

The solution of the self-consistent equations (15), (19), and (20) depends on the specific structure of the solid. Here, we will solve them for the fcc lattice, which is the structure of inert gas solids. The solution of these self-consistent equations in the case of all-neighbor interactions is presented in the Appendix. For a potential involving nearest-neighbor interactions only, we find

$$D=\frac{1}{2\beta\Delta v(d)\gamma^2\pi^3}\int_0^{\pi}\int_0^{\pi}\int_0^{\pi}[G(\mathbf{k})\coth G(\mathbf{k})-1]d^3\mathbf{k}, \quad (21)$$

where

$$G(\mathbf{k})=\hbar\beta\gamma\sqrt{\Delta v(d)/m}\,[1-\tfrac{1}{3}(\cos k_1\cos k_2+\cos k_2\cos k_3+\cos k_1\cos k_3)]^{1/2} , \quad (22)$$

and

$$\gamma^2=\frac{1}{\Delta v(d)}\sum_{L=0}^{\infty}\frac{1}{L!}\left[\frac{D}{2}\right]^L\Delta^{(L+1)}v(d) . \quad (23)$$

The nearest-neighbor distance d is adjusted to give the appropriate pressure for the system. The expression (22) for $G(\mathbf{k})$ is essentially an eigenvalue of the dynamical matrix for nearest-neighbor interactions in the fcc lattice, except that the trial action used in our theory is equivalent to using a single force constant for each interaction.

As in the one-dimensional case,[9] once the solution of

the self-consistent equations is found for the equilibrium configurations (an fcc lattice, in our case), one can calculate the first-order corrections to the eigenvalues and expand the effective potential in terms of the quantum renormalization factor D. The result is

$$V_{\text{eff}}(\bar{\mathbf{r}})=\frac{1}{2}\sum_{i\neq j}[v(\bar{\mathbf{r}}_i-\bar{\mathbf{r}}_j)+v_{\text{eff}}(\bar{\mathbf{r}}_i-\bar{\mathbf{r}}_j)] + \frac{3N}{\beta\pi^3}\int_0^{\pi}\int_0^{\pi}\int_0^{\pi}\ln\left[\frac{\sinh G(\mathbf{k})}{G(\mathbf{k})}\right]d^3\mathbf{k} , \tag{24}$$

where

$$v_{\text{eff}}(\bar{\mathbf{r}}_i-\bar{\mathbf{r}}_j)=\sum_{L=1}^{\infty}\frac{1}{L!}\left[\frac{D}{2}\right]^L \times[\Delta^{(L)}v(\bar{\mathbf{r}}_i-\bar{\mathbf{r}}_j)-L\Delta^{(L)}v(d)] . \tag{25}$$

This effective potential is fully consistent up to terms of order D^2. The usefulness of the expansion of Eqs. (23) and (25) in terms of D, of course, depends on how large D is. More specifically, the higher-order terms must be small compared with the lower-order ones. For example, taking the ratio of the second term in Eq. (23) to the first term, one gets the so-called Ginzburg parameter

$$G=\frac{1}{2}D\frac{\Delta^2 v(d)}{\Delta v(d)} .$$

If G is very small compared to 1, one needs only keep the first term in Eqs. (23) and (25). The resulting effective potential is the first-order effective potential. For a larger G, or higher accuracy, one then has to keep the second term in Eqs. (23) and (25). The resulting effective potential is called the second-order effective potential. It is clear that for the effective potential method to work, the parameter G must be less than 1. For inert gas solids, it varies from very small in the case of Xe to quite large in the case of Ne. For He, G is about 2 and so the present formalism is not suitable for that case. We plan to treat He in a separate paper. In particular, we can avoid the series expansion by using a numerical integration technique. The parameter G for Ar and Ne is plotted in Fig. 1. In general, G decreases with increasing temperature, so the effective potential method works better and better as the temperature rises. At high temperatures, the first term of the Wigner expansion[2] is recovered in this theory. At the highest temperatures, the particles have no "time" to travel at all, they must stay on their classical trajectories. The quantum fluctuations are then zero ($D=0$) and we go back to the classical case, $V_{\text{eff}}=V$. So the effective potential method is guaranteed to work at temperatures around the Debye temperature and above. Whether it can be usefully applied at lower temperatures depends on the size of the quantum effects in the system. As we will see in the next section, for solids with moderate quantum effects, the effective potential method is reliable at all temperatures!

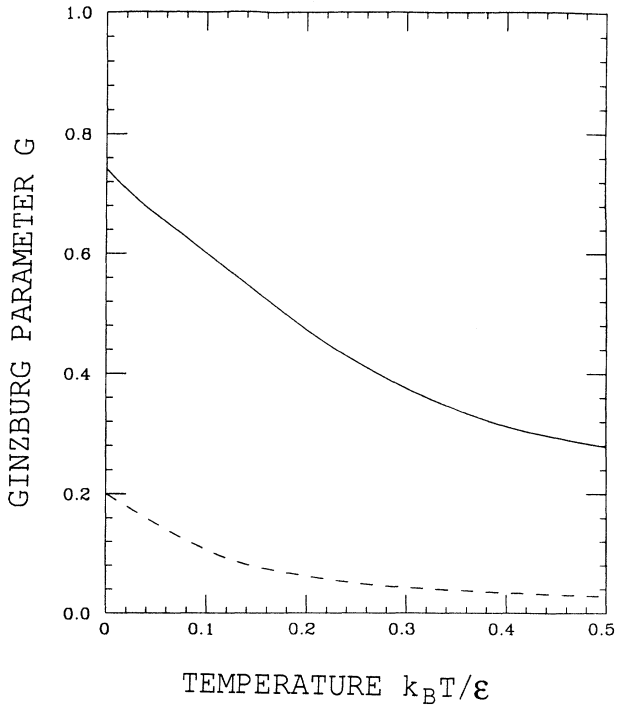

FIG. 1. The Ginsburg parameters as a function of temperature for solid Ar and ^{22}Ne (solid line).

III. DISCUSSION OF THE RESULTS FOR MLJ SOLIDS

Since Eq. (13) is of the classical form, one can use traditional classical techniques to calculate equilibrium properties. In the following, we will use the CMC technique[11] to calculate thermodynamic properties for a nearest-neighbor MLJ model of solid Xe, Kr, Ar, and ^{22}Ne (the neon isotope). Modifications are made to account for the temperature and volume dependence of the effective potential. A feature of the self-consistency requirement of the effective potential method is that the effective potential must be redetermined for each temperature and each nearest-neighbor distance.

We shall use a nearest-neighbor MLJ(12-6) potential,

$$v(r)=4\varepsilon\left[\left[\frac{\sigma}{r}\right]^{12}-\left[\frac{\sigma}{r}\right]^{6}\right] . \tag{26}$$

The quantum effects for inert gas solids are then measured by a single parameter, the de Boer parameter, $\alpha=\hbar/\sigma\sqrt{m\varepsilon}$. We list values of α along with other data for inert gas solids in Table I.

When studying MLJ solids, it is convenient to express

TABLE I. MLJ potential parameters for the inert gas solids. All data are taken from Horton (Ref. 12) except for the neon isotope in which case we use the same parameters as the ones used in Ref. 5.

	α	$\varepsilon(10^{-16}$ erg)	σ(Å)
Xe	0.008 73	452.55	3.8469
Kr	0.013 93	325.2	3.5600
Ar	0.025 51	235.95	3.3043
^{22}Ne	0.076 09	72.09	2.7012

all physical quantities in reduced units. From now on, we will express the temperature t in units of ε/k_B, internal energy per atom E in units of ε, distance d in units of σ, pressure P in units of ε/σ^3 and heat capacity per atom C_v in units of k_B. That leaves the de Boer parameter as the one species specific quantity in the formalism. The Monte Carlo calculations were done for a sample of 108 atoms with periodic boundary conditions. At each temperature, we carry out at a Monte Carlo run of 4.2 million configurations. The first 0.2 million moves were used to warm up the solids. They were then discarded. The remaining 4 million moves were then broken into 20 blocks to enable us to estimate statistical uncertainties. At each temperature, the nearest-neighbor distance is adjusted until the pressure, in reduced units, is less than 0.01. Based on the isothermal compressibility data for these solids and our test runs, the nearest-neighbor distance given here should be within 0.02% of its value at absolute zero pressure in the worst case. Our results for the nearest-neighbor distance d, for internal energy per atom E and the heat capacity per atom C_v, for the inert gas solids are shown in Figs. 2–7, and listed in Table II. For the heat capacity, the error bars in the figures corre-

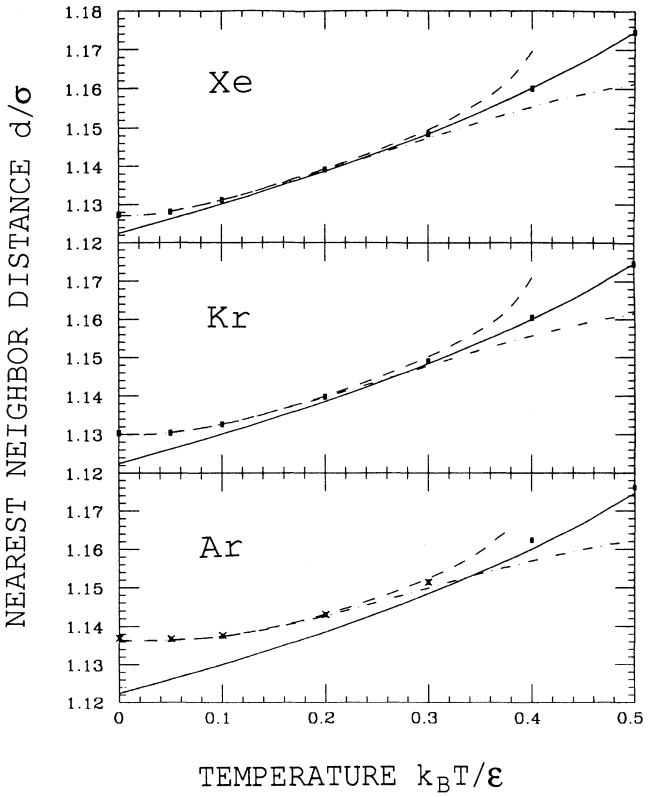

FIG. 2. Nearest-neighbor distances as a function of temperature for solid Xe, Kr, and Ar. The upper dashed lines correspond to perturbation theory to order λ^4. The lower dashed lines correspond to perturbation theory to order λ^2. The solid lines correspond to smoothed CMC results. The points are the results of the first-order effective potential method. The crosses are results of the second-order effective potential.

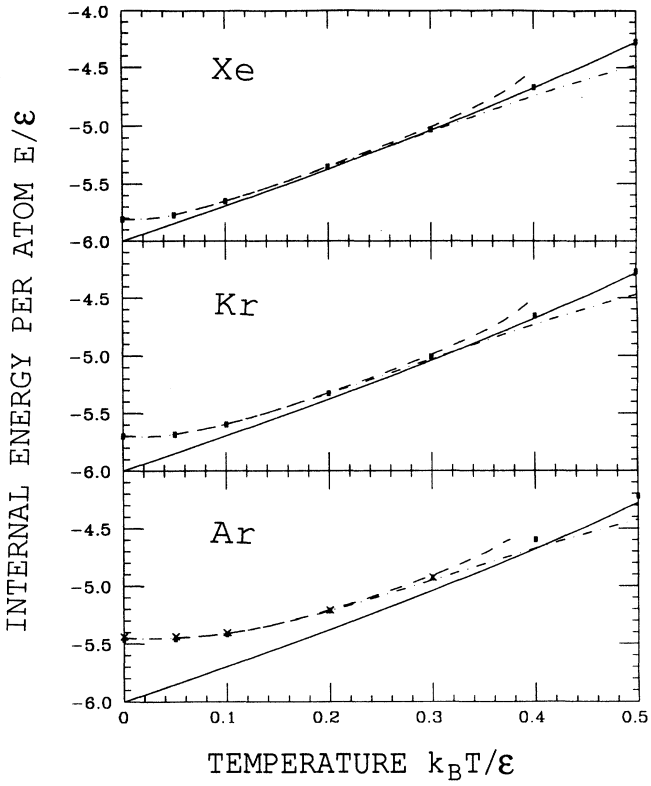

FIG. 3. Internal energies per atom as a function of temperature for solid Xe, Kr, and Ar. Other notation as in Fig. 2.

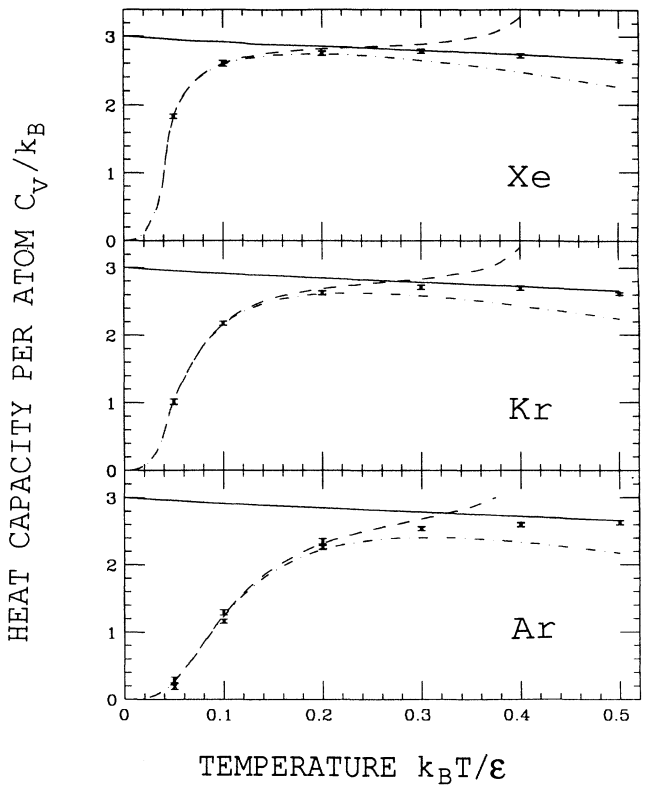

FIG. 4. Heat capacities per atom as a function of temperture for solid Xe, Kr, and Ar. Other notation as in Fig. 2.

TABLE II. Results of the Monte Carlo calculations with the effective potentials for solid Xe, Kr, Ar, and ^{22}Ne. The nearest-neighbor distances d, internal energies per atom E, heat capacities per atom C_v, pressure P, and temperatures t are all expressed in the reduced units.

t	d	E	$10^4\Delta E$	C_v	ΔC_v	10^3P	$10^3\Delta P$	t	d	E	$10^4\Delta E$	C_v	ΔC_v	10^3P	$10^3\Delta P$
		First-order effective potential results for Xe								First-order effective potential results for Kr					
0.05	1.128 1	−5.7736	1.2	1.84	0.03	−6.4	0.6	0.05	1.130 4	−5.6834	1.4	1.01	0.04	2.3	0.7
0.1	0.131 1	−5.6540	2.4	2.59	0.04	−4.0	1.3	0.1	1.132 6	−5.5971	3.0	2.18	0.03	−5.6	1.5
0.2	1.139 0	−5.3568	4.7	2.75	0.03	0.1	2.4	0.2	1.139 84	−5.3262	4.1	2.63	0.03	−1.5	2.0
0.3	1.148 4	−5.0298	6.0	2.78	0.03	8.6	2.9	0.3	1.149 1	−5.0007	8.0	2.72	0.02	5.7	4.3
0.4	1.159 9	−4.6730	5.6	2.71	0.03	3.9	2.9	0.4	1.160 4	−4.6566	8.1	2.70	0.03	4.7	4.0
0.5	1.174 54	−4.2737	11	2.64	0.02	−5.6	5.2	0.5	1.174 54	−4.2678	11	2.62	0.02	−2.7	5.2
		First-order effective potential results for Ar								Second-order effective potential results for Ar					
0.05	1.136 66	−5.4592	1	0.29	0.04	0.2	0.7		1.136 85	−5.4363	1	0.18	0.04	0.2	0.5
0.1	1.137 45	−5.4190	2	1.29	0.04	0.1	1.2		1.137 65	−5.4034	2	1.16	0.03	0.7	0.8
0.2	1.142 95	−5.2151	4	2.35	0.04	1.1	1.8		1.143	−5.2097	5	2.26	0.03	1.5	2.3
0.3	1.151 4	−4.9307	8	2.54	0.03	0.1	3.8		1.151 4	−4.9277	8	2.54	0.03	3.2	4.1
0.4	1.162 3	−4.5978	9	2.60	0.03	0.5	4.2								
0.5	1.176 1	−4.2212	12	2.63	0.03	−1.4	5.7								
		First-order effective potential results for ^{22}Ne								Second-order effective potential results for ^{22}Ne					
0.05	1.167 92	−4.5929	1	0.11	0.04	1.4	0.4		1.168 5	−4.3949	1	0.03	0.04	−2.3	0.5
0.1	1.166 5	−4.5785	3	0.45	0.04	−0.7	1.2		1.168 08	−4.3901	2	0.17	0.04	1.2	0.9
0.134	1.166 1	−4.5607	3	0.66	0.04	−2.3	1.2		1.168 16	−4.3812	4	0.32	0.03	−1.6	1.6
0.192	1.166 6	−4.5088	7	1.14	0.05	−1.9	2.6		1.168 9	−4.3524	7	0.77	0.04	−6.1	2.5
0.249	1.168 5	−4.4282	8	1.52	0.05	3.8	3.1		1.170 75	−4.2943	9	1.10	0.04	0.3	3.2
0.306	1.171 7	−4.3221	8	1.86	0.04	5.3	3.3		1.173 69	−4.2097	9	1.57	0.04	7.5	3.8
0.364	1.176 34	−4.1905	11	2.04	0.04	−2.7	4.4		1.178 05	−4.0992	11	1.86	0.05	−5.5	4.4
0.421	1.182	−4.0386	13	2.16	0.03	−2.1	5.7		1.183 4	−3.9608	12	1.97	0.04	8.5	4.6
0.5	1.192 5	−3.7835	12	2.29	0.03	8.6	4.7		1.193 7	−3.7251	16	2.17	0.04	4.7	6.3

TABLE III. Results of the effective potential methods at zero degrees. d_1 and d_2 are the nearest-neighbor distances corresponding to the first and the second-order effective potential, respectively. d_3 is the nearest-neighbor distance calculated by using the effective potential with the third terms of Eqs. (23) and (25) included. E_1, E_2, and E_3 are the corresponding internal energies per atom. All distances and energies are expressed in the reduced units.

	Xe	Kr	Ar	^{22}Ne
d_1	1.127 34	1.130 30	1.137 08	1.170 36
d_2	1.127 32	1.130 26	1.136 95	1.169 01
d_3	1.127 32	1.130 26	1.136 92	1.168 35
E_1	−5.808 9	−5.698 8	−5.463 7	−4.596 7
E_2	−5.805 9	−5.691 1	−5.438 4	−4.395 4
E_3	−5.805 8	−5.690 8	−5.437 0	−4.367 6

spond to one standard deviation. For the internal energy, the statistical uncertainties are much smaller than the size of the symbols. Though not shown in these figures, the CMC results[13] for the heat capacity have statistical uncertainties of about the same magnitude of those of the effective potential results.

Effective potential results at zero degrees are listed in Table III. These results are directly determined from the

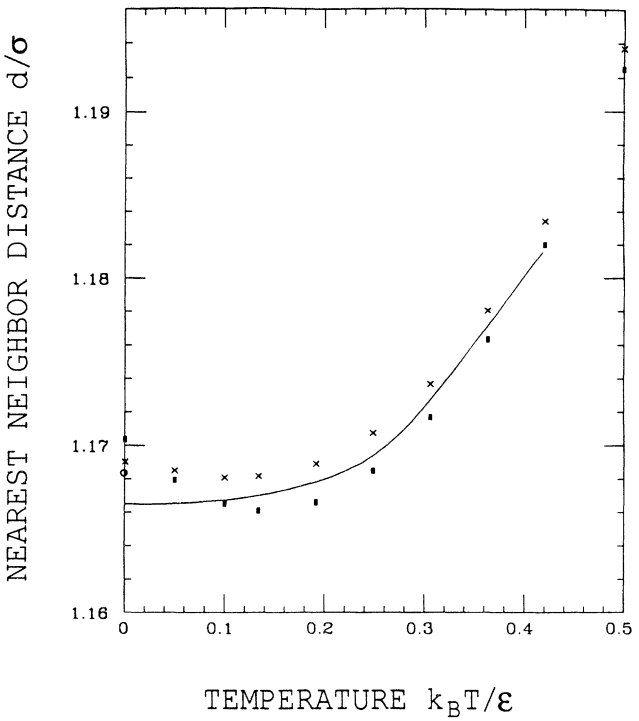

FIG. 5. Nearest-neighbor distance as a function of temperture for solid ^{22}Ne. The points and crosses are the results of the first- and second-order effective potential method, respectively. The open circle is the result of the effective potential method with the third terms of Eqs. (23) and (25) included. The solid line is the ISC result (Ref. 5).

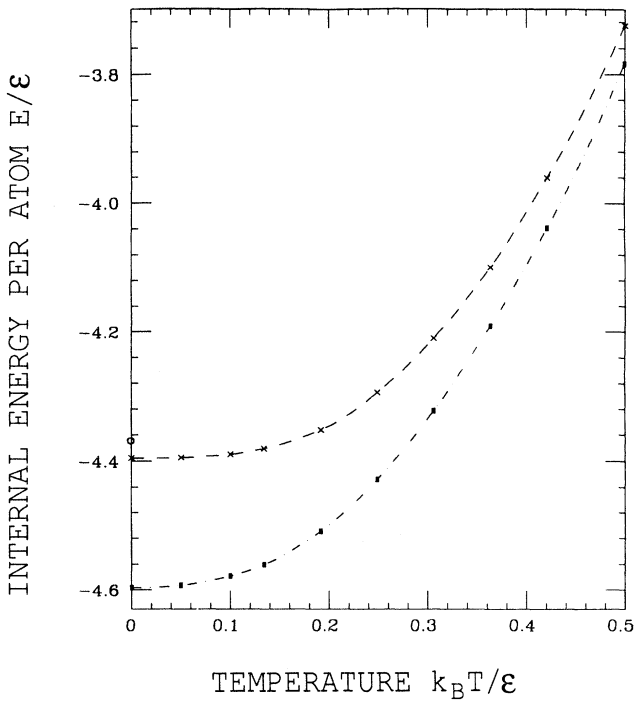

FIG. 6. Internal energy per atom as a function of temperature for solid ^{22}Ne. The upper dashed and lower dashed lines are smoothed results of the second- and the first-order effective potential method with the actual data shown as crosses and points. The open circle is the result of the effective potential method with the third terms of Eqs. (23) and (25) included.

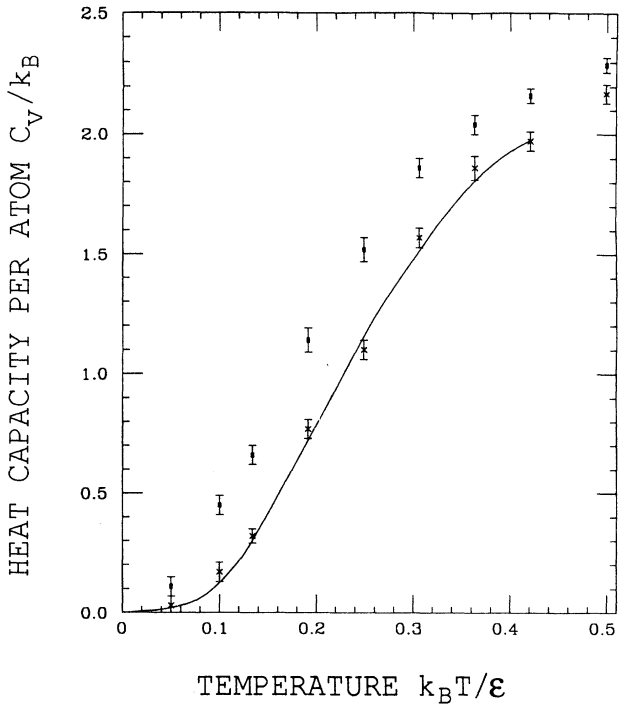

FIG. 7. Heat capacity per atom as a function of temperature for solid ^{22}Ne. Other notation as in Fig. 5.

effective potential at $T=0$. By comparing results of effective potentials of different orders, one can check the validity of the effective potential method. For example, if the corrections due to the second-order effective potential to the first-order one are small, the effective potential method is reliable. To estimate higher-order corrections, we include the third terms of Eqs. (23) and (25). Though these third terms are not fully consistent, they should give a good indication how important the third- and higher-order effective potential is. We now discuss each of the inert gas solid results individually.

A. Solid Xe and Kr

Among the inert gas solids, solid Xe and Kr show the smallest quantum effect. One would certainly expect the effective potential method to be very reliable for them. Our theory agrees remarkably well with the perturbation theory[14] at low temperatures. Based on temperatures at which the different orders of the perturbation theory diverge, the perturbation theory should be reliable up to a reduced temperature of about 0.2. Our theory also agrees with CMC at high temperatures. This is no surprise since our theory contains the CMC formalism exactly, as well as the leading quantum correction[2] to it. The present results show that solid Xe becomes classical at about $t=0.3$ and solid Kr does so at about $t=0.4$. From Table III one can see that corrections due to second- and higher-order effective potentials are negligible. The Ginzburg parameters, G, are very small for these two solids. Overall, we conclude that the theory accounts reliably for the thermal properties of these solids.

B. Solid Ar

Solid Ar exhibits moderate quantum effects. From Figs. 2–4, one can see very small corrections due to the second-order effective potential. Our theory, once again, agrees very well with the perturbation theory[14] results under conditions where they are reliable ($t \leq 0.2$). At very high temperature, our theory, as expected, approaches the CMC results. There is a small difference between the present theory and CMC at high temperatures. This is due to the fact that near the melting temperature, there are still some quantum effects present. This is understandable since for solid Ar, the Debye temperature is about the same as the melting temperature.

From Table III, one can see that the third- or higher-order corrections are negligible for Ar. As shown in Fig. 1, the parameter G is about 0.2 at $t=0$. The ratio of the third term of Eq. (23) to the second term at $t=0$, is, however, 0.018. This also means that higher-order corrections are not important.

C. Solid ^{22}Ne

Solid Ne has such large zero-point vibrations that theories based on a perturbation expansion diverge even at zero degrees. The improved self-consistent (ISC) theory[5] was used to account for such large zero-point vibrations. It is not clear, however, how reliable ISC really is. The big difference between the second- and the first-order effective potential also reflects the fact that solid Ne exhibits large quantum effects, as one can see from Fig. 1, the parameter G is quite large ($G=0.7$, at $t=0$). However, the ratio of the third term of Eq. (23) to the second term is 0.19, at $t=0$. This suggests that the third-order correction for Ne is of the same order as the second-order corrections for Ar. The third-order results at $t=0$ also show this. The first-order effective potential actually gives a large negative thermal expansion at very low temperature. The situation is much improved by the second-order corrections. Though we do not have the fully consistent third- and higher-order effective potentials, we believe that will add a small correction to eliminate this problem, as Fig. 5 indicates. Thus, we believe, the second-order results for Ne are quite reliable, especially at high temperatures. In comparison with ISC, our present theory gives about the same heat capacity, but somewhat larger nearest-neighbor distances.

It is also clear from studying solid Ne that the effective potential method will become unreliable for systems with larger quantum effects such as solid He. Further refinements are needed.

To summarize, the theory presented in this paper accounts reliably both for quantum effects and large thermal vibrations. It is reliable at all temperatures for systems with a large range of quantum effects. Since most solids are of this kind, we believe the effective potential method will have wide applications and offer an advantageous alternative to the quantum Monte Carlo (QMC) approach for these solids. This is important, because, using QMC to obtain reliable values of higher-order derivatives of the free energy, such as the heat capacity, has proved to be very difficult.[15,16] On the other hand, more work needs to be done to make the effective potential method applicable to systems with very large quantum effects, such as solid He.

ACKNOWLEDGMENTS

We would like to thank A. A. Maradudin, A. McGurn, R. Vaia, Z. Zhu, and Z. Gong for helpful discussions. This work was partially supported by NSF under Grant No. DMR-88-08756 and the Pittsburgh Supercomputing Center under Grant No. DMR890022P. We thank the Rutgers University Research Council for a supportive grant.

APPENDIX: SOLUTION OF THE SELF-CONSISTENT EQUATIONS

The key point is to find an orthogonal matrix U to diagonalize Eq. (20). We will use three indexes $(i_1,i_2,i_3)=i$ to label the ith atom positioned at $i_1\mathbf{a}_1+i_2a_2+i_3\mathbf{a}_3$, where $\mathbf{a}_1,\mathbf{a}_2$, and $\mathbf{a}_2$ are the three base vectors. For an fcc lattice, one has $\mathbf{a}_1=(d/\sqrt{2})(1,1,0),\mathbf{a}_2=(d/\sqrt{2})(1,0,1)$ and $\mathbf{a}_1=(d/\sqrt{2})(0,1,1)$, where d is the nearest-neighbor distance. The condition that the ith and the jth atoms are the nearest neighbors is

$$b_{1,i,j}=\delta_{i_1,j_1+1}\delta_{i_2j_2}\delta_{i_3j_3}+\delta_{i_2,j_2+1}\delta_{i_1j_1}\delta_{i_3j_3}+\delta_{i_3,j_3+1}\delta_{i_1j_1}\delta_{i_2j_2}$$
$$+\delta_{i_1,j_1-1}\delta_{i_2j_2}\delta_{i_3j_3}+\delta_{i_2,j_2-1}\delta_{i_1j_1}\delta_{i_3j_3}+\delta_{i_3,j_3-1}\delta_{i_1j_1}\delta_{i_2j_2}$$
$$+\delta_{i_1,j_1+1}\delta_{i_2,j_2-1}\delta_{i_3j_3}+\delta_{i_1,j_1-1}\delta_{i_2,j_2+1}\delta_{i_3j_3}+\delta_{i_1j_1}\delta_{i_2,j_2+1}\delta_{i_3,j_3-1}$$
$$+\delta_{i_1j_1}\delta_{i_2,j_2-1}\delta_{i_3,j_3+1}+\delta_{i_1,j_1+1}\delta_{i_2j_2}\delta_{i_3,j_3-1}+\delta_{i_1,j_1-1}\delta_{i_2j_2}\delta_{i_3,j_3+1}\ . \tag{A1}$$

The question now becomes to find the U matrix which diagonalizes Eq. (A1). The answer is

$$U_{ij}=U_{i_1i_2i_3,j_1j_2j_3}=U_{i_1,j_2j_3}\otimes U_{i_2,j_1j_3}\otimes U_{i_3,j_1j_2}\ , \tag{A2}$$

where

$$U_{i_1,j_2,j_3}=\begin{cases}\left[\frac{2}{2M+1}\right]^{1/2}\cos\frac{2\pi i_1(j_2+j_3)}{2M+1}, & -M\le i_1\le -1\\ \left[\frac{1}{2M+1}\right]^{1/2}, & i_1=0\\ \left[\frac{2}{2M+1}\right]^{1/2}\sin\frac{2\pi i_2(j_3+j_1)}{2M+1}, & 1\le i_1\le M\ ,\end{cases} \tag{A3}$$

$$U_{i_2,j_3j_1}=\begin{cases}\left[\frac{2}{2M+1}\right]^{1/2}\cos\frac{2\pi i_2(j_3+j_1)}{2M+1}, & -M\le i_2\le -1\\ \left[\frac{1}{2M+1}\right]^{1/2}, & i_2=0\\ \left[\frac{2}{2M+1}\right]^{1/2}\sin\frac{2\pi i_2(j_3+j_1)}{2M+1}, & 1\le i_2\le M\ ,\end{cases} \tag{A4}$$

and

$$U_{i_3,j_1j_2}=\begin{cases}\left[\frac{2}{2M+1}\right]^{1/2}\cos\frac{2\pi i_3(j_1+j_2)}{2M+1}, & -M\le i_3\le -1\\ \left[\frac{1}{2M+1}\right]^{1/2}, & i_3=0\\ \left[\frac{2}{2M+1}\right]^{1/2}\sin\frac{2\pi i_3(j_1+j_2)}{2M+1}, & 1\le i_3\le M\ ,\end{cases} \tag{A5}$$

In Eq. (A2), $\otimes$ means the direct product and the number of atoms $N=(2M+1)^3$. In the continuous limit, M will be taken to be infinite. It is easy to check that the U matrix given by Eq. (A2) is orthogonal and it diagonalizes Eq. (A1). The result is

$$U_{ki}(h_1-b_{1,i,j})U_{k'j}=12Q^2(k)\delta_{kk'}\ , \tag{A6}$$

where

$$Q^2(k)=1-\frac{1}{3}\left[\cos\left[\frac{2\pi k_1}{2M+1}\right]\cos\left[\frac{2\pi k_2}{2M+1}\right]+\cos\left[\frac{2\pi k_2}{2M+1}\right]\cos\left[\frac{2\pi k_3}{2M+1}\right]+\cos\left[\frac{2\pi k_1}{2M+1}\right]\cos\left[\frac{2\pi k_3}{2M+1}\right]\right]\ . \tag{A7}$$

Substituting Eq. (A2) into Eqs. (15) and (19), one gets

$$f_k^2=\frac{\beta^2}{m}Q^2(k)\sum_{L=0}^{\infty}\frac{1}{L!}\left[\frac{D}{2}\right]^L\Delta^{(L+1)}v(d)\ , \tag{A8}$$

and

$$D(d)=\frac{1}{N}\sum_{k=1}^{N}\alpha_k Q^2(k)\ . \tag{A9}$$

In the continuous limit $M\to\infty$, the summations over k will be replaced by integration. One then gets Eqs. (21) and (22).

The U matrix given by Eq. (A2) can actually diagonalize all $b_{n,i,j}$ at the same time. Let $n_1=j_1-i_1$, $n_2=j_2-i_2$, and $n_2=j_3-i_3$. For a potential involving all-neighbor interactions, we then find

$$f_k^2=\frac{\beta^2}{m}\sum_n \frac{h_2}{12}Q_n^2(k)\sum_{L=0}^{\infty}\frac{1}{L!}\left[\frac{D_n}{2}\right]^L \Delta^{(L+1)}v(d_n). \tag{A10}$$

For an fcc lattice, we have

$$Q_n^2(k)=1-\frac{1}{h_n}\sum_{(n_1,n_2,n_3)}\cos\left[\frac{2\pi(n_2+n_3)k_1}{2M+1}\right]\cos\left[\frac{2\pi(n_1+n_3)k_2}{2M+1}\right]\cos\left[\frac{2\pi(n_1+n_2)k_3}{2M+1}\right] \tag{A11}$$

and

$$D_n=\frac{1}{N}\sum_{k=1}^{N}\alpha_k Q_n^2(k)\ . \tag{A12}$$

In Eq. (A11), the summation is over all the nth-neighbor atoms.

[1]See, for example, M. Born and K. Huang, *Dynamical Theory of Crystal Lattices* (Clarendon Press, Oxford, 1954); *Dynamical Properties of Solids,* edited by G. K. Horton and A. A. Maradudin (North-Holland, Amsterdam, 1975), Vol. 2.

[2]E. P. Wigner, Phys. Rev. **40**, 749 (1932).

[3]P. F. Choquard, *The Anharmonic Crystals* (Benjamin, New York, 1967); V. Samathiyakanit and H. R. Glyde, J. Phys. C **6**, 1166 (1973).

[4]E. R. Cowley and G. K. Horton, Phys. Rev. Lett. **58**, 789 (1987).

[5]V. V. Goldman, G. K. Horton, and M. L. Klein, Phys. Rev. Lett. **21**, 1527 (1968); J. Low Temp. Phys. **1**, 391 (1969).

[6]R. Giachetti and V. Tognetti, Phys. Rev. Lett. **55**, 912 (1985); Phys. Rev. B **33**, 7647 (1986).

[7]R. P. Feynman and H. Kleinert, Phys. Rev. A **34**, 5080 (1986).

[8]R. P. Feynman and A. R. Hibbs, *Quantum Mechanics and Path Integrals* (McGraw Hill, New York, 1965).

[9]A. Cuccoli, V. Tognetti, and R. Vaia, Phys. Rev. B **41**, 9588 (1990).

[10]S. Liu, G. K. Horton, and E. R. Cowley, Phys. Lett. A **152**, 79 (1991).

[11]N. Metropolis, A. W. Rosenbluth, M. N. Rosenbluth, A. H. Teller, and E. Teller, J. Chem. Phys. **21**, 1087 (1953).

[12]G. K. Horton, in *Rare Gas Solids,* edited by M. L. Klein and J. A. Venables (Academic, New York, 1976).

[13]E. R. Cowley, Phys. Rev. B **28**, 3160 (1983).

[14]R. C. Shukla and E. R. Cowley, Phys. Rev. B **31**, 372 (1985) and unpublished results.

[15]A. R. McGurn, P. Ryan, A. A. Maradudin, and R. F. Wallis, Phys. Rev. B **40**, 2407 (1989).

[16]A. R. McGurn and A. A. Maradudin (private communication).